CPP

Contributions to Plasma Physics

www.cpp-journal.org

WILEY-VCH

REPRINT

Contrib. Plasma Phys. **52**, No. 10, 856 – 863 (2012) / **DOI** 10.1002/ctpp.201200032

Wall Charge and Potential from a Microscopic Point of View

F. X. Bronold[*], **H. Fehske, R. L. Heinisch,** and **J. Marbach**

Institut für Physik, Ernst-Moritz-Arndt-Universität Greifswald, D-17487 Greifswald, Germany

Received 29 April 2012, accepted 20 June 2012
Published online 08 November 2012

Key words Plasma-wall interaction, wall charge, secondary electron emission

Macroscopic objects floating in an ionized gas (plasma walls) accumulate electrons more efficiently than ions because the influx of electrons outruns the influx of ions. The floating potential acquired by plasma walls is thus negative with respect to the plasma potential. Until now plasma walls are typically treated as perfect absorbers for electrons and ions, irrespective of the microphysics at the surface responsible for charge deposition and extraction. This crude description, sufficient for present day technological plasmas, will run into problems in solid-state based gas discharges where, with continuing miniaturization, the wall becomes an integral part of the plasma device and the charge transfer across it has to be modelled more precisely. The purpose of this paper is to review our work, where we questioned the perfect absorber model and initiated a microscopic description of the charge transfer across plasma walls, put it into perspective, and indicate directions for future research.

1 Introduction

All low-temperature gas discharges are bound by macroscopic objects. In contrast to magnetically confined, high-temperature plasmas they strongly interact with solids which either operate as electrodes, providing the break-down voltage, or simply as floating walls, preventing the constituents of the plasma to disappear. The most fundamental manifestation of the solid-plasma interaction is the plasma sheath adjacent to an unbiased, floating wall. It is an intrinsic electron-depleted region which solely arises because the plasma is bound by a solid [1].

The sheath is the macroscopic indication of a microscopic charge transfer across the plasma wall. Electrons are deposited in and extracted from the wall until a negative wall potential results which repels electrons and attracts ions such that quasi-stationarity of the potential can be maintained. The microscopic understanding of this process is rather rudimentary. Usually, it is assumed that all electrons and ions hitting the wall annihilate instantly which is the same as to say that the wall is a perfect absorber and that at the wall the electron and ion influx balance. Most of the modeling of gas discharges (see, for instance, Loffhagen and Sigeneger [2] for a recent review) uses this boundary condition and leaves thus no room for the description of the charge transfer across the plasma wall. At best the wall is characterized by an electron-ion recombination coefficient and secondary electron emission coefficients for various impacting species.

Clearly, the perfect absorber model implicitly assumes that for the phenomena occurring in the discharge the time and spatial scales of the charge transfer across the plasma wall are irrelevant and hence there is no need to track them [1]. How electrons are trapped in or at the wall, what their binding energy and residence time is, how and from what kind of electronic states they are released, and how the sheath potential merges with the surface potential of the wall are beyond the scope of this crude modeling of the plasma wall. In various novel bounded plasmas [3] it seems to be however rewarding to pay more attention to these questions. In dusty plasmas [4–8], for instance, the total amount of charge soaked up by the dust particles affects of course the overall characteristic of the discharge [9] and should thus be known as precisely as possible. Likewise it is by now also well known [10–14] that the wall charge plays an active role in determining the spatio-temporal structure of dielectric barrier discharges [15] and microplasmas [16, 17]. A detailed understanding of the charge transfer across the plasma-dielectric interface promises therefore an improved control of this type of discharges.

[*] Corresponding author. E-mail: bronold@physik.uni-greifswald.de

Finally and most fascinating, in solid-state based microdischarges [18, 19], the (biased) plasma wall becomes with continuing miniaturization even an integral part of the discharge and thus needs to be explicitly modelled.

Inspired by Emeleus and Coulter [20] as well as Behnke and coworkers [10, 21] who attempted to describe the dynamics of the wall charge and its coupling to the bulk plasma with phenomenological rate equations, characterized by sticking coefficients, residence times, and recombination and emission coefficients, we initiated in the framework of the TRR24 an effort to describe the plasma wall beyond the perfect absorber model [22–24]. With an eye on grain charging in dusty plasmas and the wall charge in dielectric barrier discharges we calculated – as a first step – for various uncharged metallic [23] and dielectric [25–27] surfaces electron sticking coefficients and desorption times, determined the distribution of the wall charge across the interface between a plasma and a floating dielectric surface [28], and investigated how electrons are extracted from dielectric surfaces via de-exciting metastable molecules [29, 30]. Below we discuss the status of our work, put it into perspective, and indicate where it should go in the future.

2 Build-up of the wall charge: Deposition of electrons

In contrast to the assumptions of the perfect absorber model, an electron impinging on a solid surface is either reflected, inelastically scattered, or temporarily deposited to the surface. Possible trapping states (or sites) and hence residence times and penetration depths depend on its energy, the inelastic coupling to the elementary excitations of the surface driving energy relaxation, and the work function (electron affinity) of the material.

The surface physics just described can be encoded in a Hamiltonian. For a planar surface, with a potential which varies only perpendicularly to the surface, and using the eigenstates of this potential as a basis [23],

$$H = \sum_q E_q c_q^\dagger c_q + \sum_s E_s d_s^\dagger d_s + \sum_{s,q,q'} \langle q|\hat{V}_s|q'\rangle c_q^\dagger c_{q'} \ , \tag{1}$$

where the first term describes the motion of the impinging electron in the surface potential, the second term denotes the motion of the elementary excitations of the wall responsible for energy relaxation, and the last term is the coupling of these excitations to the electron; q and s label the respective states and excitations.

The basis in which the Hamiltonian is written down, the elementary excitations causing energy relaxation, and the coupling $\hat{V}_s$ depend on the surface. Below we show results for dielectric surfaces where the elementary excitations are acoustic phonons and the surface potential is a truncated image potential. This model is applicable to a dielectric surface with negative electron affinity, that is, a dielectric where the bottom of the conduction band is above the potential just outside the surface, MgO and LiF being two important examples. For such a surface image states are stable and can thus host the approaching electron. In order to investigate the dependence of the trapping scenario on material parameters, for instance, the Debye frequency and the dielectric function, and to show trends we applied the model however also to dielectric materials with positive electron affinity [25–27].

In analogy to physisorption of neutral particles [31] we take the time evolution of the occupancy of bound surface states labelled by n as a measure for temporary trapping. It satisfies a rate equation [25–27],

$$\frac{\mathrm{d}n_n(t)}{\mathrm{d}t} = \sum_{n'} \left[W_{nn'} n_{n'}(t) - W_{n'n} n_n(t)\right] - \sum_k W_{kn} n_n(t) + \sum_k \tau_t W_{nk} j_k \ , \tag{2}$$

where the transition probabilities $W_{...}$ have to be calculated from (1), j_k denotes the stationary flux corresponding to a single electron in the unbound surface state k, and $\tau_t = 2L/v_z$ is the traveling time through the surface region where energy relaxation occurs. For relaxation happening in external surface states, the length L can be absorbed in the transition probabilities and drops out in the limit $L \to \infty$ which can be meaningfully taken in this case. If however energy relaxation takes place inside the wall, as in dielectrics with positive electron affinity, L is the penetration depth and has to be obtained from experiments or theoretically calculated [24].

A quantity characterizing trapping of an electron with wave number k is the prompt sticking coefficient [31],

$$s_{e,k}^{\text{prompt}} = \tau_t \sum_n W_{nk} \ , \tag{3}$$

which is the probability to make during one round trip in the relevant surface region a transition from an unbound to a bound state. In case the surface potential supports only one bound state this is enough and the rate equation (2)

is not needed. If however the surface potential supports many bound states and the elementary excitations causing energy relaxation are not energetic enough to connect the lowest bound state directly with unbound states, the characterization of trapping has to be based on the rate equation. From its slowly varying part [31],

$$\frac{\mathrm{d}n^{\mathrm{slow}}(t)}{\mathrm{d}t} = \sum_k s^{\mathrm{kin}}_{e,k} j_k(t) - \frac{1}{\tau_e} n^{\mathrm{slow}}(t)\,, \tag{4}$$

the residence or desorption time τ_e and the kinetic sticking coefficient $s^{\mathrm{kin}}_{e,k}$, which is the probability for trapping and relaxation of an electron with wave number k in the manifold of bound surface states, can then be extracted.

We applied the approach just outlined to various uncharged dielectric surfaces assuming electron physisorption to occur in the image potential, which is, as pointed out, rigorously true only for dielectrics with negative electron affinity [25–27]. Electron energy relaxation at these surfaces is driven by acoustic phonons whose Debye energy is very often not only too small to connect the lowest bound state to the unbound states but also too small to connect the two lowest bound states. The physisorption kinetics of electrons at dielectric surfaces involves therefore multiphonon transitions [25–27]. Only the initial trapping of electrons in the upper bound states, characterized by the prompt sticking coefficient, occurs via one-phonon processes. Multiphonon processes contribute very little to it. Hence, initial trapping is rather insensitive to the surface temperature. Relaxation after initial trapping depends on the strength of transitions from the upper bound states to the lowest bound state. If the lowest two bound states are linked by a one-phonon transition, a trapped electron relaxes for all surface temperatures, if a multiphonon process is required, the electron relaxes only for low temperatures whereas for room temperature and higher relaxation is inhibited leading to a relaxation bottleneck. The dominant desorption channel depends also on the depth of the potential. For a shallow potential desorption occurs directly from the lowest bound state to the continuum. For deeper potentials desorption proceeds via the upper bound states. Desorption occurs then via a cascade in systems without and as a one-way process in systems with relaxation bottleneck [27].

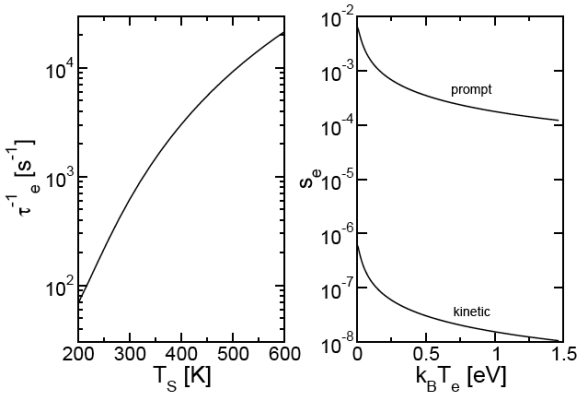

Fig. 1 Inverse of the electron residence time as a function of the surface temperature T_s for an electron thermalized with a LiF surface (left panel) and $k-$averaged prompt and kinetic sticking coefficients (right panel) for an electron approaching a LiF surface at $T_s = 300K$ with a kinetic energy which is Boltzmann distributed over the unbound surface states with average energy $k_B T_e$. The perfect absorber model implies $s_e = 1$ and $\tau_e^{-1} = 0$.

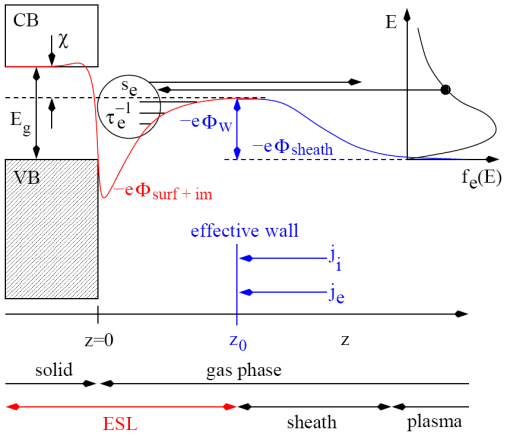

Fig. 2 Energetic situation in front of a dielectric surface with $\chi < 0$ and $-e\phi_w > 0$. The red line is the graded interface potential on which the model of an electron surface layer (ESL) is based. Also shown is the electron energy distribution function in the plasma, the effective wall where the flux balance condition is enforced, and the image states where the electrons comprising the wall charge get trapped.

Electron physisorption at an uncharged dielectric surface is thus an intriguing phenomenon. For the plasma context most important is that $s_e \ll 1$ and $\tau_e^{-1} \neq 0$ [25–27], implying that an initially uncharged dielectric surface with a negative electron affinity is not a perfect absorber for electrons. Representative results for LiF are shown in Fig. 1. Since the wall charge does not affect the relative line up of the potential just outside the dielectric and the bottom of the conduction band (potential just inside the dielectric), as mistakenly assumed in [24] but corrected in [28], this conclusion also holds for a charged dielectric wall with negative electron affinity. The

sticking coefficient is only larger and thus closer to the value implied by the perfect absorber model when the electron affinity is positive and the impinging electron enters the wall, that is, for materials with positive electron affinity. In such a case the residence time should be also much longer, as implied by the perfect absorber model.

After the initial charge-up is completed, the wall carries a quasi-stationary negative charge, that is, in the notation of electron physisorption, a quasi-stationary electron adsorbate. We will now discuss how the spatial profile of the electron adsorbate normal to the crystallographic interface can be determined. The basic idea [28] is to use a graded interface potential [32] to interpolate between the sheath and the wall potential and to distribute the surplus electrons making up the wall charge in this potential under the assumption that at quasi-stationarity they are thermalized with the wall [33]. For the present purpose it suffices to describe qualitatively the simplest implementation of this idea – the crude electron surface layer (see Fig. 2 and [28]).

The adsorbed electrons form an interface-specific electron distribution – the electron surface layer – across the planar interface at $z = 0$. Their spatial profile $n(z)$ can be calculated as follows [28]. (i) First, an effective wall has to be defined. Its position, $z_0 > 0$, marks the point where the sheath merges with the electron surface layer. For $z > z_0$ electrons are repelled back into the plasma, whereas for $z < z_0$ electrons are pushed towards the surface. Hence, a flux balance is taken at z_0. Moreover, the field strength at z_0 due to the positive sheath charge is related to the total number of surplus electrons per unit area N. In order to calculate z_0 and the field strength at z_0 a sheath model and a flux balance condition are required. The results presented in Fig. 3 and discussed below, for instance, are – for simplicity – based on a collisionless sheath with a perfect absorber condition at z_0. (ii) Second, equations for the electron distribution $n(z)$ and the potential $\phi(z)$ in the electron surface layer, that is, for $z < z_0$ have to be set-up. For that purpose, density functional theory can be employed [33]. The central equation is then given by minimizing the grand canonical potential of the interacting surplus electrons in the external potential provided by the surface and the sheath. In the local density approximation, it reads [28]

$$-e(\phi_{\rm im}(z) + \phi_{\rm surf}(z) + \phi_{\rm C}(z)) + \mu^h(n(z), T_s) - \mu = 0 \,, \tag{5}$$

where $\mu^h(n(z), T_s)$ is the chemical potential of a homogeneous electron gas with density $n(z)$ at the surface temperature T_s, $\phi_{\rm im}(z)$ is the graded image potential, $\phi_{\rm surf}(z)$ is the graded surface potential accounting for the electron affinity of the surface, that is, the offset of the potential just outside the dielectric and the bottom of the conduction band (see Fig. 2), and $\phi_{\rm C}(z)$ is the Coulomb potential satisfying the Poisson equation,

$$\frac{\rm d}{{\rm d}z}\left(\epsilon(z)\frac{\rm d}{{\rm d}z}\phi_{\rm C}(z)\right) = 4\pi e n(z) \,, \tag{6}$$

with $\epsilon(z)$ the graded dielectric constant interpolating between the dielectric constants of the plasma and the dielectric. The total potential $\phi(z) = \phi_{\rm im}(z) + \phi_{\rm surf}(z) + \phi_{\rm C}(z)$ and μ is the chemical potential of the surplus electrons. (iii) Third, Eq. (5) has to be solved iteratively (until μ is stationary) subject to the boundary condition described in (i) and the additional constraint $\int_{z_0}^{z_s} {\rm d}z\, n(z) = N$ which guarantees charge neutrality between the electron surface layer and the plasma sheath. In the crude electron surface layer $z_s < 0$ is a cut-off which has to be chosen large enough in order not to affect the numerical results. In the refined electron surface layer it is the point where the electron surface layer merges with the intrinsic region of the dielectric [28].

In Fig. 3 we show results for two floating dielectric walls in contact with a helium discharge with plasma density $n_0 = 10^7 cm^{-3}$ and electron temperature $k_B T_e = 2eV$. The numerical calculations were performed as described in Ref. [28]. Depending on the electron affinity χ the distribution of electrons at the surface assumes two distinct forms: For LiF ($\chi < 0$), the conduction band minimum lies above the potential just outside and the surplus electrons are bound in the image potential in front of the wall forming an external, very narrow surface charge which can be regarded as the quasi two-dimensional electron gas anticipated by Emeleus and Coulter [20]. Its spatial profile does not change much with surface temperature and surface density of electrons (depending on the plasma parameters). For Al_2O_3 ($\chi > 0$), the conduction band minimum lies below the potential just outside and the surplus electrons accumulate inside the dielectric forming an internal wall charge. Increasing the surface density of electrons (through the plasma parameters) makes the electron distribution more concentrated at the interface (steeple-like) while at higher surface temperature it is more extended. Also shown in Fig. 3 are the potential, the electron density, and the ion density in the sheath. The latter two are discontinuous at z_0 because inside the electron surface layer electron and ion fluxes are neglected. For further discussion see Ref. [28].

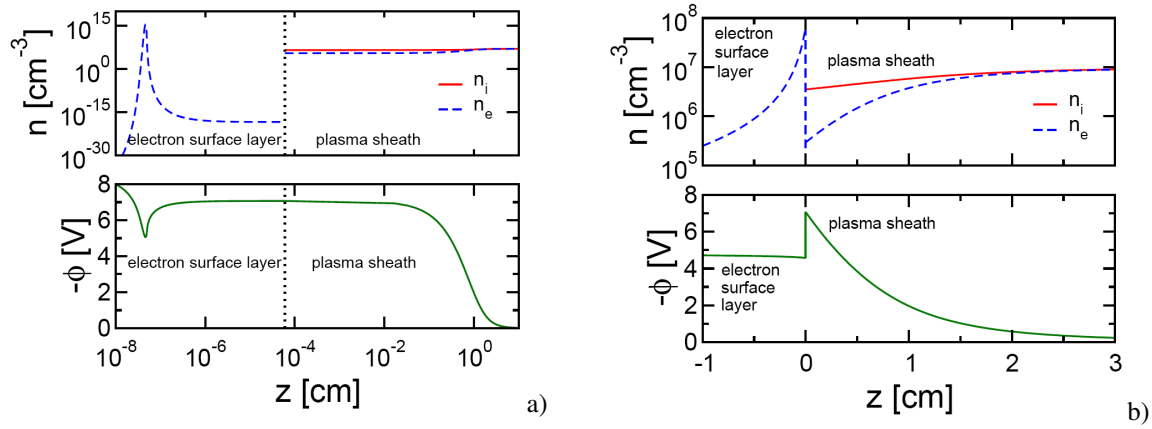

Fig. 3 Density of plasma-supplied surplus electrons trapped in the ESL, electron and ion density in the plasma sheath, and electric potential for a LiF (panel **a**) and an Al_2O_3 surface (panel **b**) in contact with a helium discharge with plasma parameters $n_0 = 10^7 cm^{-3}$ and $k_B T_e = 2eV$. The crystallographic interface is at $z = 0$. Note, the different scales of the two panels. The deep penetration of the Al_2O_3 wall charge is due to the neglect of defect states and other collision centers.

The model of an electron surface layer is an attempt to describe that part of the plasma boundary which leaks into the plasma wall. It provides a way to determine the distribution and binding energy of the wall charge as well as the spatial profile of the potential inside the wall. We described the electron surface layer for a floating wall but it can be generalized to a biased wall as well, that is, an electrode by simply supplementing it by an external bias.

3 Tapping the charge of the wall: Extraction of electrons

We now turn our attention to the extraction of electrons from the wall. The most important process extracting electrons from the wall is the wall recombination of positive ions. But high energy electrons and metastable molecules or radicals carrying internal energy are also very efficient in releasing electrons from the wall.

In the following we will focus on secondary electron emission from dielectric walls due to metastable nitrogen molecules. This process, which has been shown to stabilize the diffusive mode of dielectric barrier discharges [12], plays an important role in an in-house experimental effort to obtain, via surface and volume diagnostics, a complete characterization of such discharges, comprising volume as well as surface processes [14].

An important parameter for the modeling of dielectric barrier discharges is the secondary electron emission coefficient, characterizing the efficiency with which electrons can be extracted from the dielectric coverage of the electrode. It depends on the surface material, the projectile, and the particular collision process. For $N_2(^3\Sigma_u^+)$ two de-excitation channels [34] can provide an additional electron for the discharge. The molecule either de-excites via an Auger process corresponding to the reaction (possible at metallic surfaces [29])

$$N_2(^3\Sigma_u^+) + e_{\vec{k}} \rightarrow N_2(^1\Sigma_g^+) + e_{\vec{q}}\,, \tag{7}$$

with $e_{\vec{k}}$ and $e_{\vec{q}}$ denoting a surface electron and a free electron, respectively, or via a resonant electron capture leading to a negatively charged shape resonance, $N_2^-(^2\Pi_g)$, which subsequently decays corresponding to

$$N_2(^3\Sigma_u^+) + e_{\vec{k}} \rightarrow N_2^-(^2\Pi_g) \rightarrow N_2(^1\Sigma_g^+) + e_{\vec{q}}\,. \tag{8}$$

For most dielectrics the Auger process is energetically suppressed, diamond being an important exception (see Fig. 4**a**). The combination of charge capture and subsequent decay of the negative ion (surface-induced as well as natural via auto-detachment) is thus the dominant de-excitation channel for $N_2(^3\Sigma_u^+)$ at dielectric surfaces [30].

The reaction chain (8) consists of two sequential resonant tunneling processes (see Fig. 4**a**): resonant charge transfer (RCT) and auto-detachment (AuD). Each step can be modelled by an Anderson-Newns Hamiltonian [35], which is an effective model, stripped of some of the microscopic details and characterized instead by a small

number of material parameters which can be easily obtained. Models of this type are well suited for describing elementary processes at plasma walls where the lack of surface diagnostics prevents a more refined modeling. The Hamiltonian appropriate for (8) reads

$$H(t) = \sum_{\vec{k}} \varepsilon_{\vec{k}}\, c^{\dagger}_{\vec{k}}\, c_{\vec{k}} + \varepsilon_m(t)\, c^{\dagger}_m\, c_m + \sum_{\vec{k}} \left(V_{\vec{k}}(t)\, c^{\dagger}_{\vec{k}}\, c_m + V^{*}_{\vec{k}}(t)\, c^{\dagger}_m\, c_{\vec{k}} \right) \ , \tag{9}$$

where, for the first (second) step of the reaction chain $\vec{k}$ denotes electronic states within the solid's valence band (free electron states) and m labels the lower (upper) ionization level of the negative shape resonance $N_2^-(^2\Pi_g)$. Using Keldysh Green functions [36] it is possible to calculate from (9) the rate for resonant electron capture $\Gamma_0(t)$ and the rate for surface-induced decay $\Gamma_{\rm surf}(t)$. For details see Ref. [30].

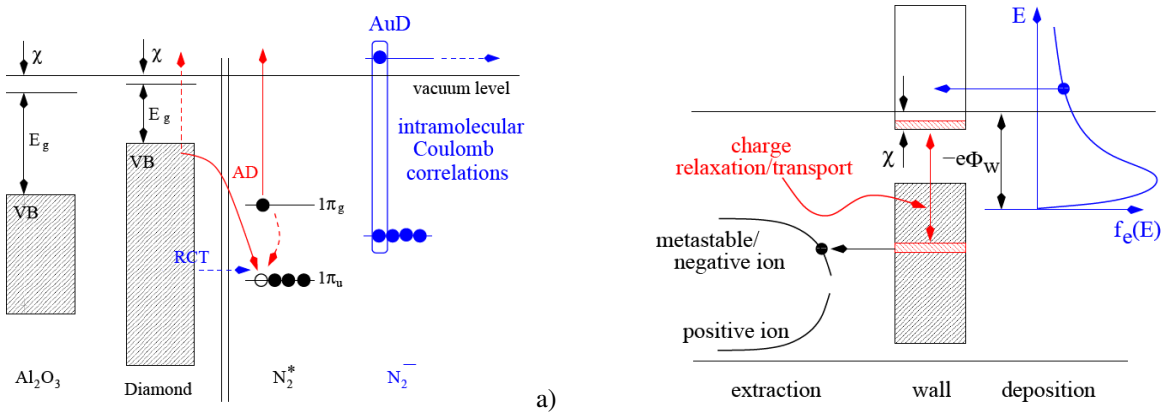

Fig. 4 **a**) Energy scheme showing for a $N_2(^3\Sigma_u^+)$ molecule scattering off a diamond and Al_2O_3 surface direct (red dashed) and indirect (red solid) Auger de-excitation (AD) and resonant charge transfer (RCT) with subsequent auto-detachment (AuD) of the $N_2^-(^2\Pi_g)$ shape resonance (dashed blue). **b**) Illustration of the energetic situation for electron deposition and extraction at a dielectric plasma wall with positive electron affinity. The electrons deposited in the conduction band of the solid are qualitatively shown as well as the holes in the valence band arising from the extraction of electrons by positive ions and/or metastables/negative ions. The inversion of the occupancy of the states in the dielectric may persist only temporarily until it is eliminated by charge relaxation and transport or radiative processes.

The ionization levels $\varepsilon_m(t)$ and the tunnel matrix element $V_{\vec{k}}(t)$ depend on time via the molecule's position relative to the surface. Assuming, for simplicity, normal incidence, and the molecule to start moving at $t_0 = -\infty$ and to hit the surface at $t = 0$, the trajectory of the molecule's center of mass is $\vec{R}(t) = z_R(t)\,\vec{e}_z = (v_0\,|t| + z_1)\,\vec{e}_z$, where z_1 is the turning point in the surface potential of the molecule and v_0 is the molecule's velocity. Explicit expressions for the matrix elements appearing in (9) can be found in Ref. [30]. In Fig. 4**a** we show the relevant ionization levels of $N_2(^3\Sigma_u^+)$ and $N_2^-(^2\Pi_g)$ for $t_0 = -\infty$. Note, due to intra-molecular Coulomb correlations the ionization levels of $N_2^-(^2\Pi_g)$ are shifted with respect to the ones of $N_2(^3\Sigma_u^+)$. In accordance to the fact that $N_2^-(^2\Pi_g)$ is an unstable shape resonance, the upper ionization level of $N_2^-(^2\Pi_g)$ is above the vacuum level. The rate for the natural decay $\Gamma_{\rm nat}$ can be deduced from the life time assuming a Breit-Wigner-type line shape for the auto-ionization process [30].

Relating the occupancies of the lower ($m = 0$) and the upper ionization level ($m = 1$) of $N_2^-(^2\Pi_g)$ to the fractions of metastable molecules $n_*(t)$, negative ions $n_-(t)$, and ground state molecules $n_g(t)$, reaction (8) can be coded into a system of ordinary differential equations whose solution gives [30],

$$n_*(t) = e^{-\int_{t_0}^{t} {\rm d}t_1\ \Gamma_0(t_1)} \ , \ n_-(t) = -\int_{t_0}^{t} {\rm d}t_1\ \frac{{\rm d}n_*(t_1)}{{\rm d}t_1}\ e^{-\int_{t_1}^{t} {\rm d}t_2\ \Gamma_1(t_2)} \ , \tag{10}$$

where $\Gamma_1 = \Gamma_{\rm surf} + \Gamma_{\rm nat}$ is the total decay rate containing the surface-induced and the natural decay. The fraction of ground state molecules follows from $n_g(t) = 1 - n_*(t) - n_-(t)$. Writing the total decay rate Γ_1 in terms of an energy spectral function [30] we also obtain the probability of emitting an electron,

$$n(t) = \int_0^{\infty} {\rm d}\varepsilon_{\vec{q}}^{\infty} \int_{t_0}^{t} {\rm d}t_1\ \varrho_1(\varepsilon_{\vec{q}}^{\infty}, t_1)\, n_-(t_1) \ , \tag{11}$$

which defines the secondary electron emission coefficient, $\gamma_e = n(\infty)$, as well as the energy spectrum of the emitted electron, $\mathrm{d}n(\infty)/\mathrm{d}\varepsilon_{\vec{q}}^{\infty}$. Here $\varepsilon_{\vec{q}}^{\infty}$ denotes the energy of the electron far away from the surface.

Using the above formalism we investigated for various dielectric surfaces the de-excitation of $N_2(^3\Sigma_u^+)$ via reaction (8) [30]. Figure 5 shows results for a SiO_2 surface. The spectrum of the emitted electron is shown in Fig. 5**a**. The kinetic energy of the molecule is $50\,meV$ and only the natural decay was taken into account because it dominates the surface-induced decay by one order of magnitude [30]. The cut-off of the spectrum at low energy arises from the trapping of the emitted electron in the image potential when its perpendicular kinetic energy is too small. The secondary electron emission coefficient γ_e is shown in Fig. 5**b** as a function of the molecule's kinetic energy ε_{kin}. The inset, finally, depicts for a molecular kinetic energy of $50\,meV$ the time evolution of the fraction of metastables n_* and ground state molecules n_g. These data demonstrate clearly that due to the fast decay of $N_2^-(^2\Pi_g)$ the decrease of $n_*(t)$ leads to an almost instantaneous increase of $n_g(t)$ by the same amount and thus to a very efficient release of an electron.

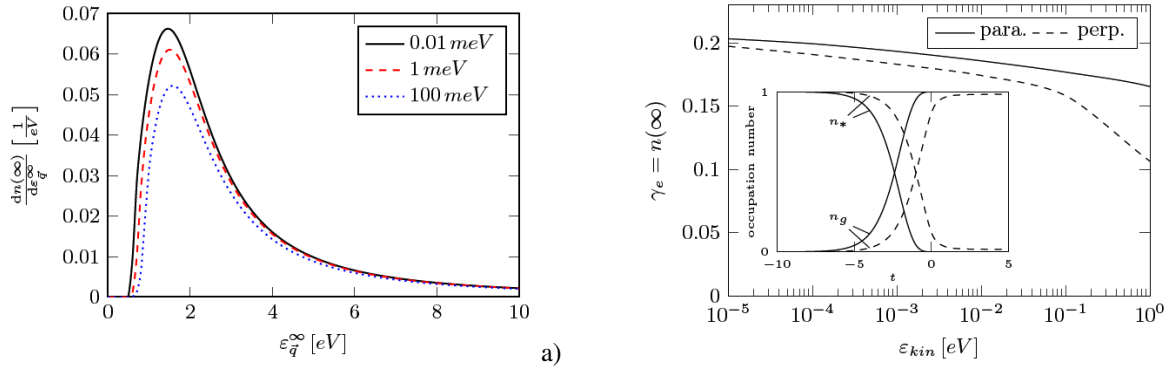

Fig. 5 **a**) Spectrum of the electron emitted from a SiO_2 surface upon impact of a metastable $N_2(^3\Sigma_u^+)$ molecule with perpendicular molecular axis and three different kinetic energies. **b**) Secondary electron emission coefficient γ_e due to de-exciting $N_2(^3\Sigma_u^+)$ at an SiO_2 surface as a function of the molecule's kinetic energy and the two orientations of the molecular axis. The inset shows the time evolution ($t < 0$ incoming and $t > 0$ outgoing branch of the trajectory) of the fractions of the metastables n_* and ground state molecules n_g.

It is interesting to note that the de-excitation of $N_2(^3\Sigma_u^+)$ extracts an electron from the valence band whereas the wall charge would reside in the conduction band of SiO_2 (see Fig. 4**b** for an illustration). The charge transfer due to the build-up of the wall charge, on the one hand, and the de-excitation of $N_2(^3\Sigma_u^+)$, on the other, thus leads to an inversion of the band occupancies. The time and length scales on which it persists until it is eliminated by radiative processes or electron relaxation and transport are not yet explored. Support for this microscopic picture comes however from measurements of the wall charge in dielectric barrier discharges which indicate the presence of positive wall charges [14]. From our perspective, these are holes in the dielectric's valence band.

4 Concluding remarks

In a still on-going effort we question the perfect absorber model for plasma walls and develop concepts and tools for a microscopic description of the interaction of electrons and other species with plasma walls. We are particularly interested in how electrons are deposited in and extracted from floating plasma walls and how they are distributed across the plasma-wall interface once a quasi-stationary floating potential is established.

So far, we mostly considered uncharged metallic and dielectric surfaces but our results already indicate that floating dielectric plasma walls with negative electron affinity cannot be described as perfect absorbers because $s_e \ll 1$, irrespective of the charge of the surface. Our results also indicate that in this case the wall charge forms a quasi two-dimensional electron film in front of the surface. The total charge collected by a plasma wall most probably does not depend on whether it is trapped in front or inside the wall; but knowing where the charge resides may be useful for developing diagnostics of the wall charge. The time scale, in contrast, on which the quasi-stationary wall charge develops should depend on the way it is trapped. A time-resolved study of, for instance, charging and de-charging of grains in a plasma (or an electro-static trap) could thus reveal

further insights into the microphysics of wall charges. As yet unexplored is the electronic inversion temporarily existing in a floating dielectric wall because the electron influx deposits electrons in the conduction band (or in unoccupied surface states, depending on the electron affinity), and the influx of ions and/or metastables extracts electrons from the valence band. We focused on charge extraction due to metastable nitrogen but the inversion also arises due to wall recombination of positive ions. It is thus generic for a floating dielectric wall and should be investigated in detail, particularly in connection with discharges gliding on floating dielectric surfaces [14] where the build-up and decay of the inversion could affect, for instance, the spatio-temporal evolution of the discharge.

Fundamental to any interface is charge transfer. This mantra also holds for plasma walls although the rich microphysics associated with it reveals itself only after a judicious design of the wall and the discharge. The progress in manufacturing solid-state based microdischarges is therefore particularly encouraging. We used the electron surface layer to describe a floating plasma wall. Supplemented by an external bias, it can be however also used for a microscopic description of biased walls, for instance, the plasma bipolar junction transistor [18], where the plasma wall is an integral part of the device.

Acknowledgements Support from the Deutsche Forschungsgemeinschaft through the TRR 24 is greatly acknowledged. J. M. was funded by the federal state of Mecklenburg-Western Pomerania through a postgraduate scholarship.

References

[1] R.N. Franklin, Plasma phenomena in gas discharges (Clarendon Press, Oxford, 1976).
[2] D. Loffhagen and F. Sigeneger, Plasma Sources Sci. Technol. **18**, 034006 (2009).
[3] J. Meichsner, A. Piel, M. Bonitz, and H. Fehske, Contrib. Plasma Phys. **52**, 789 (2012).
[4] H. Baumgartner, D. Block, and M. Bonitz, Contrib. Plasma Phys. **49**, 281 (2009).
[5] A. Piel, O. Arp, D. Block, I. Pilch, T. Trottenberg, S. Kaeding, A. Melzer, H. Baumgartner, C. Henning, and M. Bonitz, Plasma Phys. Control. Fusion **49**, 281 (2008).
[6] V.E. Fortov, A.V. Ivlev, S.A. Khrapak, A.G. Khrapak, and G.E. Morfill, Physics Reports **421**, 1 (2005).
[7] M. Bonitz et al., Contrib. Plasma Phys. **52**, 890 (2012).
[8] G. Schubert et al., Contrib. Plasma Phys. **52**, 827 (2012).
[9] J. Berndt, E. Kovacevic, V. Selenin, I. Stefanovic, and J. Winter, Plasma Sources Sci. Technol. **15**, 18 (2006).
[10] Y.B. Golubovskii, V.A. Maiorov, J. Behnke, and J.F. Behnke, J. Phys. D: Appl. Phys. **35**, 751 (2002).
[11] H.E. Wagner, Y.V. Yurgelenas, and R. Brandenburg, Plasma Phys. Control. Fusion **47**, B641 (2005).
[12] R. Brandenburg, V.A. Maiorov, Y.B. Golubovskii, H.E. Wagner, J. Behnke, and J. F. Behnke, J. Phys. D: Appl. Phys. **38**, 2187 (2005).
[13] L. Stollenwerk, J.G. Laven, and H.G. Purwins, Phys. Rev. Lett. **98**, 255001 (2007).
[14] M. Bogaczyk et al., Contrib. Plasma Phys. **52**, 847 (2012).
[15] U. Kogelschatz, Plasma Chemistry and Plasma Processing **23**, 1 (2003).
[16] K.H. Becker, K.H. Schoenbach, and J.G. Eden, J. Phys. D: Appl. Phys. **39**, R55 (2006).
[17] M.J. Kushner, J. Phys. D: Appl. Phys. **38**, 1633 (2005).
[18] P.A. Tchertchian, C.J. Wagner, T.J.H. Jr., B. Li, D.J. Sievers, and J.G. Eden, Contrib. Plasma Phys. **51**, 889 (2011).
[19] R. Dussart, L.J. Overzet, P. Lefaucheux, T. Dufour, M. Kulsreshath, M.A. Mandra, T. Tillocher, O. Aubry, S. Dozias, P. Ranson, J.B. Lee, and M. Goeckner, Eur. Phys. J. D **60**, 601 (2010).
[20] K.G. Emeleus and J.R.M. Coulter, Int. J. Electronics **62**, 225 (1987).
[21] J.F. Behnke, T. Bindemann, H. Deutsch, and K. Becker, Contrib. Plasma Phys. **37**, 345 (1997).
[22] F.X. Bronold, H. Fehske, H. Kersten, and H. Deutsch, Phys. Rev. Lett. **101**, 175002 (2008).
[23] F.X. Bronold, H. Deutsch, and H. Fehske, Eur. Phys. J. D **54**, 519 (2009).
[24] F.X. Bronold, R.L. Heinisch, J. Marbach, and H. Fehske, IEEE Transactions on Plasma Science **39**, 644 (2011).
[25] R.L. Heinisch, F.X. Bronold, and H. Fehske, Phys. Rev. B **81**, 155420 (2010).
[26] R.L. Heinisch, F.X. Bronold, and H. Fehske, Phys. Rev. B **82**, 125408 (2010).
[27] R.L. Heinisch, F.X. Bronold, and H. Fehske, Phys. Rev. B **83**, 195407 (2011).
[28] R.L. Heinisch, F.X. Bronold, and H. Fehske, Phys. Rev. B **85**, 075323 (2012).
[29] J. Marbach, F.X. Bronold, and H. Fehske, Phys. Rev. B **84**, 085443 (2011).
[30] J. Marbach, F.X. Bronold, and H. Fehske, Eur. Phys. J. D **66**, 106 (2012).
[31] H.J. Kreuzer and Z.W. Gortel, Physisorption Kinetics (Springer Verlag, Berlin, 1986).
[32] F. Stern, Phys. Rev. B **17**, 5009 (1978).
[33] E.E. Tkharev and A.L. Danilyuk, Vacuum **35**, 183 (1985).
[34] P. Stracke, F. Wiegershaus, S. Krischok, and V. Kempter, Surface Science **396**, 212220 (1998).
[35] A. Yoshimori and K. Makoshi, Progress in Surface Science **21**, 251294 (1986).
[36] A. Blandin, A. Nourtier, and D.W. Hone, J. Phys. France **37**, 369 (1976).

